

Analysis of three-neutrino oscillations in the full mixing angle space

D. C. Latimer and D. J. Ernst

Department of Physics and Astronomy, Vanderbilt University, Nashville, Tennessee 37235, USA

(Dated: December 2, 2024)

We construct a model, with no CP violation, of the world's neutrino oscillation data, excluding the LSND experiments, and search the full parameter space ($0 \leq \theta_{12} \leq \pi/2$; $-\pi/2 \leq \theta_{13} \leq \pi/2$; and $0 \leq \theta_{23} \leq \pi/2$) for the best fit values of the mixing angles and mass-squared differences. We find θ_{13} and Δm_{21}^2 highly correlated and bounded by $-0.11 < \theta_{13} < 0.08$ and $2.8 \times 10^{-5} \text{ eV}^2 < \Delta m_{21}^2 < 5.1 \times 10^{-5} \text{ eV}^2$. Note that negative θ_{13} is physical and that oscillation probabilities are dependent on the sign of θ_{13} . The χ^2 -space for small negative θ_{13} is found to have two competing valleys. The remaining parameters are found to have values, $\theta_{12} \approx 0.57$, $\theta_{23} \approx 0.50$, and $\Delta m_{32}^2 \approx 2.5 \times 10^{-3} \text{ eV}^2$. The model dependent analysis presented here strongly motivates a further examination of the negative θ_{13} region, a region heretofore overlooked.

PACS numbers: 14.60.-z, 14.60.Pq

Keywords: neutrino, oscillations, three neutrinos, neutrino mixing

The observation of neutrino oscillations requires a fundamental modification of the electroweak theory. The simplest, but not totally consistent, method for accommodating neutrino oscillations into the theory is to in-

duce *a posteriori* a mass matrix and unitary mixing matrix. The standard Maiani [1] representation of the three neutrino mixing matrix is

$$U_{\alpha k} \rightarrow \begin{pmatrix} c_{12}c_{13} & s_{12}c_{13} & s_{13}e^{-i\delta} \\ -s_{12}c_{23} - c_{12}s_{23}s_{13}e^{i\delta} & c_{12}c_{23} - s_{12}s_{23}s_{13}e^{i\delta} & s_{23}c_{13} \\ s_{12}s_{23} - c_{12}c_{23}s_{13}e^{i\delta} & -c_{12}s_{23} - s_{12}c_{23}s_{13}e^{i\delta} & c_{23}c_{13} \end{pmatrix}, \quad (1)$$

where $c_{\alpha k} = \cos \theta_{\alpha k}$, $s_{\alpha k} = \sin \theta_{\alpha k}$, and δ is the CP violating phase with $\theta_{\alpha k}$ and δ real. We order the mass eigenstates by increasing mass, and the flavor eigenstates are ordered electron, mu, tau. The bounds on the mixing angles θ_{jk} are $0 \leq \theta_{jk} \leq \pi/2$ and $0 \leq \delta < 2\pi$. In the absence of CP violation, the range of the mixing angles [2] is $0 \leq \theta_{jk} \leq \pi/2$ with $\delta = 0$ and $\delta = \pi$; or equivalently [3] one may consider *only* $\delta = 0$ and allow *either* θ_{12} or θ_{23} to be bounded by $0 \leq \theta_{jk} < \pi$; or equivalently [3] take *only* $\delta = 0$ and $0 \leq \theta_{12} \leq \pi/2$, $-\pi/2 \leq \theta_{13} \leq \pi/2$, and $0 \leq \theta_{23} \leq \pi/2$. The third option is the most convenient as experiments indicate that θ_{13} is near zero. As we have used option two previously, we note that $(\theta_{12}, \theta_{13}, \theta_{23}) \equiv (\theta_{12}, -\theta_{13}, \pi - \theta_{23})$ maps option two onto option three. In particular, oscillation probabilities for θ_{13} negative are not related to those for θ_{13} positive. Parameterization of oscillation solutions by $\sin^2 \theta_{13}$ is thus inadequate.

In vacuo, the probability that a neutrino with energy E and flavor α will be detected a distance L away as a neutrino of flavor β is given by

$$\begin{aligned} \mathcal{P}_{\alpha\beta}(L/E) &= \delta_{\alpha\beta} \\ &- 4 \sum_{\substack{j,k=1 \\ j < k}}^3 U_{\alpha j} U_{\beta j} U_{\alpha k} U_{\beta k} \sin^2 \phi_{jk}^{osc}, \end{aligned} \quad (2)$$

in which $\phi_{jk}^{osc} = 1.27 \Delta m_{jk}^2 L/E$ with L/E expressed in units of m/MeV and $\Delta m_{jk}^2 \equiv m_j^2 - m_k^2$ in units of eV². This probability is then to be integrated over the energy spectrum of the neutrinos for each experiment.

We construct a model of the data and then, within the model, look for best fit oscillation parameters throughout the full range of permitted mixing angles. Included in the model are data for neutrinos from the sun [4, 5, 6, 7, 8, 9], reactor neutrinos [10, 11], atmospheric neutrinos [12, 13], and beam-stop neutrinos [14]. We, like others, omit from the analysis the LSND [15] and Karmen [16] experiments.

Experiments for solar neutrinos [4, 5, 6, 7] historically measured the survival probability of electron neutrinos, \mathcal{P}_{ee} . Recent experiments [8, 9] measure two different neutrino interactions which then allow the extraction of \mathcal{P}_{ee} and the total solar neutrino flux. The measured total is in agreement with the theoretical predictions of the standard solar model [17]. We here use the standard solar model for the production of neutrinos in the sun. Each detector measuring solar neutrinos has a different acceptance and thus measures different energy neutrinos. In order to reproduce the energy dependence of the survival rate of electron neutrinos arriving at the Earth as seen in the experiments, we invoke the MSW effect [18]. The MSW effect arises because the neutrinos created in

the sun propagate through a medium with a significant electron density. The forward coherent elastic neutrino-electron scattering produces an effective change, relative to the mu and tau neutrino, in the mass of the electron neutrino given by $A(r) = \sqrt{2} G E \rho(r)/m_n$, with $\rho(r)$ the electron density at a radius r , G the weak coupling constant, and m_n the nucleon mass. In the flavor basis, the Hamiltonian then becomes

$$H_{mat} = U \mathcal{M} U^\dagger + A(r), \quad (3)$$

with \mathcal{M} the (diagonal) mass-squared matrix in the mass eigenstate basis and A the 3×3 matrix with the interaction $A(r)$ as the electron-electron matrix element and zeroes elsewhere. By diagonalizing this Hamiltonian with a unitary transformation $D_{\alpha k}(r, E)$, we define local masses and eigenstates as a function of r and E . Care must be taken so that $D_{\alpha k}(r, E)$ becomes $U_{\alpha k}$ in the limit of zero electron density. In the adiabatic limit, which we use, the electron survival probability is

$$P_{ee}^{ad}(r, E) = \sum_{k=1}^3 D(r, E)_{ek}^2 U_{ek}^2. \quad (4)$$

Neutrinos are produced throughout the sun by various reactions, each with its own energy spectrum. The surviving neutrinos are then detected by detectors which have a different acceptance for each energy of the neutrino. The survival probability for an electron neutrino in a particular experiment is given by

$$P_{ee}^{ex} = \sum_{j=1}^N p_j^{ex} \int_0^{R_\odot} f_j(r) dr \int_{E_{thresh}}^\infty g_j(E) P_{ee}^{ad}(r, E) dE. \quad (5)$$

Here, j labels a particular nuclear reaction; we include three reactions – pp, ${}^7\text{Be}$, and ${}^8\text{B}$. The quantity p_j^{ex} is the probability that in a particular experiment the neutrino arose from nuclear reaction j . We take these from the analysis of Ref. [19] for the solar experiments: chlorine [4], gallium (Sage, Gallex, and GNO) [5, 6, 7], SNO [8], and SNO-salt [9]. The function $f_j(r)$ is the probability that a neutrino is created by reaction j at a radius r [17] of the sun and is integrated from the center of the sun to the solar radius. The function $g_j(E)$ is the energy distribution of the neutrinos emitted in reaction j . For ${}^7\text{Be}$ this is a delta function at 0.88 MeV; the lower emission line does not contribute significantly. For the pp neutrinos, the energy distribution times the detector acceptance is a relatively narrow function of energy; we set E to its average. For ${}^8\text{B}$ neutrinos, we use the energy distribution from the standard solar model [17] and numerically perform the integration.

For three neutrino mixing, the energy dependence of the solar data is well reproduced by the MSW effect without level crossing. This is true of all the parameter sets

Experiment	Measured	L/E (m/MeV)	Data
Chlorine	\mathcal{P}_{ee}	4.0×10^{10}	$.337 \pm .065$
Gallium	\mathcal{P}_{ee}	$35. \times 10^{10}$	$.550 \pm .048$
SNO	\mathcal{P}_{ee}	2.2×10^{10}	$.348 \pm .073$
SNO-salt	\mathcal{P}_{ee}	2.2×10^{10}	$.306 \pm .035$
CHOOZ	\mathcal{P}_{ee}	300.	> 0.96
KamLAND	\mathcal{P}_{ee}	4.1×10^4	$.611 \pm .094$
K2K	$\mathcal{P}_{\mu\mu}$	208.	$.550 \pm .190$

TABLE I: The experiment, quantity measured, the average value of L/E , and experimental data for those quantities fit by the model are presented.

examined here. The adiabatic approximation is thus justified after the fact.

The reactor experiments that we include are CHOOZ [10] and KamLAND [11]. KamLAND is unique among reactor experiments as it measures \mathcal{P}_{ee} where its predecessors set limits on $1 - \mathcal{P}_{ee}$. We also include the K2K experiment [14] that measures the survival of muon neutrinos $\mathcal{P}_{\mu\mu}$ over a long baseline (250 km) from KEK to the Super-K detector. The experiment, quantity measured, the value of that quantity to which we fit, and the average value of L/E for each experiment are given in Table I.

The Super-Kamiokande experiment [12, 13] has measured neutrinos that originate from cosmic rays hitting the upper atmosphere. The detector distinguishes between e -like (electron and anti-electron) neutrinos and μ -like (muon and anti-muon) neutrinos. The rate of e -like neutrinos of energy E arriving at the detector from a source a distance L away is

$$\mathcal{R}_e(L, E) = \mathcal{P}_{ee}(L, E) + n(E) \mathcal{P}_{e\mu}(L, E), \quad (6)$$

and for μ -like neutrinos

$$\mathcal{R}_\mu(L, E) = \mathcal{P}_{\mu\mu}(L, E) + \frac{1}{n(E)} \mathcal{P}_{e\mu}(L, E), \quad (7)$$

where $n(E)$ is the ratio of μ -like neutrinos to e -like neutrinos at the source. We incorporate the Super-K atmospheric neutrinos into our analysis by utilizing the L/E -dependence of \mathcal{R}_e and \mathcal{R}_μ given in [12] and pictured in Fig. 1. We take $n(E)$ to be energy independent and equal to 2.15. As the absolute flux of cosmic rays striking the atmosphere is not known to within 15%, we introduce as a fit parameter an energy-independent renormalization factor N_{norm} that multiplies the experimental values of \mathcal{R}_e and \mathcal{R}_μ .

The ratios \mathcal{R}_e and \mathcal{R}_μ are convenient for the theorist as these are easily calculable. However, utilizing the results presented in Ref. [12] neglects the more recent [13] atmospheric data from Super-K. A distinct advantage of the atmospheric data is that for the neutrinos arriving from directly overhead to those arriving from the opposite side of the Earth, the value of L/E changes by almost

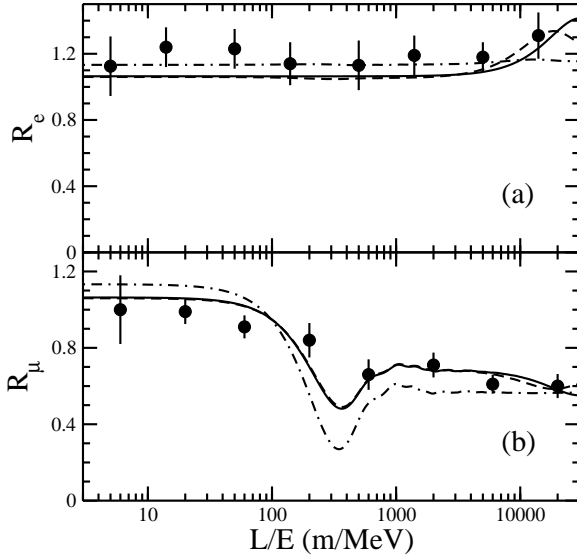


FIG. 1: Data and fits for the Super-K atmospheric experiment: (a) electron-like and (b) muon-like events. Data is represented by points. Fit 1 yields the solid line; fit 2, the dashed line; and SS, the dashed-dotted line. Here, the theory has been renormalized by N_{norm}^{-1} .

parameter\fit	SS	#1	#2
χ^2_{dof}	—	.80	.81
θ_{12}	.58	.56	.53
θ_{13}	.09	-.01	-.07
θ_{23}	.80	.50	.50
$\Delta m_{21}^2 \times 10^{-5}(\text{eV})^2$	7.0	3.0	4.9
$\Delta m_{32}^2 \times 10^{-3}(\text{eV})^2$	2.6	2.5	2.5
N_{norm}	—	.94	.94

TABLE II: The value of χ^2_{dof} and the parameters for the standard solution (SS) and the two local minima found here.

four orders of magnitude. This is the only data which varies L/E . On the other hand, the source of neutrinos from cosmic rays hitting the atmosphere must be modeled. Also, the relationship between the direction of the recoil electrons in the detector and the direction of the neutrino initiating the reaction requires additional modeling. Thus the connection between the quantity measured and a simple physical parameterization is indirect and difficult to incorporate.

We fit the mixing angles, the mass squared differences, and N_{norm} to the quantities in Table I and to the L/E dependence of \mathcal{R}_e and \mathcal{R}_μ pictured in Fig. 1 by minimizing chi-squared per degree of freedom χ^2_{dof} . In Table II, we present the parameters from the analyses of Refs. [20, 21], termed the standard solution and labeled SS, and for the two local minima in the χ^2 -space which we have found. Note that $\theta_{13} < 0$ for the minima. We have found a large number of other local minima but these all have χ^2 large enough that they are statistically eliminated.

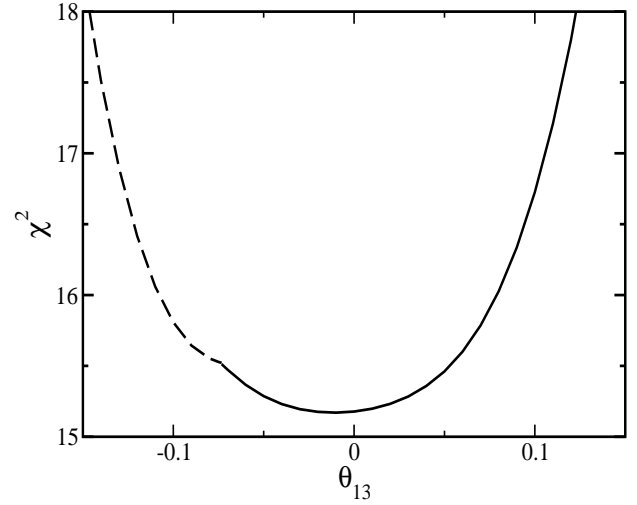


FIG. 2: The value of χ^2 for a fixed value of θ_{13} with all other parameters varied. The dashed curve represents one valley in the χ^2 -space, while the solid curve represents a second valley. The transition which occurs near $\theta_{13} = -.07$ is characterized by a finite discontinuity in Δm_{21}^2 .

Experiment	Data	SS	#1	#2
Chlorine	$.337 \pm .065$.43	.36	.39
Gallium	$.550 \pm .048$.54	.54	.57
SNO	$.348 \pm .075$.38	.31	.32
SNO-salt	$.306 \pm .035$.38	.31	.32
CHOOZ	$> .96$.99	1.00	.99
KamLAND	$.611 \pm .094$.57	.59	.61
K2K	$.550 \pm .109$.32	.54	.55

TABLE III: The experimental results and the predictions for each from the models whose parameters are given in Table II.

In Table III we compare the data with the results of the fits, and in Fig. 1 we depict the L/E dependence of each fit as compared to the atmospheric data. Fig. 1 demonstrates what we believe to be the limitation to our model. The standard solution fits in detail the Super-K data. The difference between the dashed-dot line and the data is an indication of the model dependence of our work. All three results fit well the solar and KamLAND results. In all the solutions, KamLAND is asymptotic for the large mass squared differences but ϕ^{osc} is between $\pi/2$ and π for the small mass squared difference. The K2K experiment prefers the larger value for $\mathcal{P}_{\mu\mu}$ that emerges from our two solutions. The K2K experiment is for all solutions located such that ϕ^{osc} is about 0.2π for the large mass-squared difference.

To further understand the origin of the two minima, we fix θ_{13} and minimize χ^2 under the variation of the other parameters. The results are pictured in Fig. 2. There are two valleys in the χ^2 -space in this region. Starting at θ_{13} maximally negative and increasing its value, the minimum follows a valley characterized by large and de-

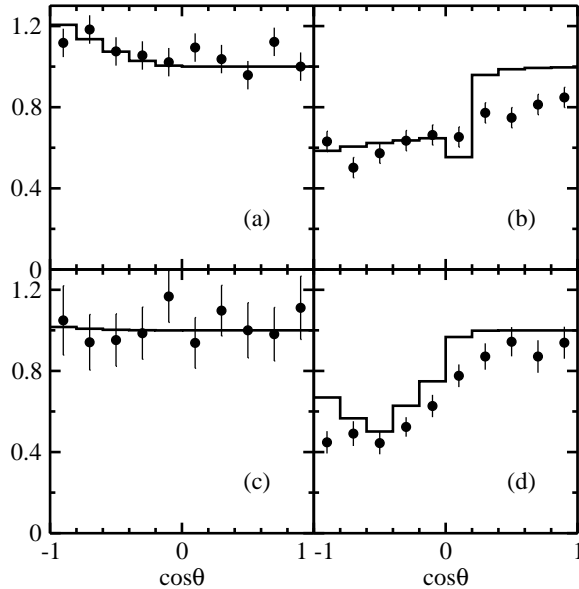


FIG. 3: Zenith-angle distributions for atmospheric Super-K experiment. Points represent the data, and the solid line shows the results of Fit 1. (a) Sub-GeV electron-like. (b) Sub-GeV muon-like. (c) Multi-GeV electron-like. (d) Multi-GeV muon-like and PC events.

creasing value of Δm_{21}^2 and nearly constant values for the other parameters. This part of the curve in Fig. 2 is dashed. At $\theta_{13} = -0.07$ the absolute minimum for this valley is found and nearly simultaneously the global minimum moves to a second valley. This transition is characterized by a finite discontinuity in Δm_{21}^2 while the other parameters continue unchanged. The absolute minimum of this second valley occurs at $\theta_{13} = -0.01$. The part of the curve arising from this valley in Fig. 2 is depicted by a solid line. Note that the valley depicted by the dashed line does not continue on to positive values of θ_{13} .

In order to further demonstrate that our results are reasonable, we also calculate the zenith-angle dependence of the atmospheric data. Using the energies defined for the various classes of neutrino events in [13], we determine \mathcal{R}_e and \mathcal{R}_μ for 10 bins ranging from downward going ($\cos \theta = 1$) to upward going ($\cos \theta = -1$) neutrinos. We also allow for a simple, but more realistic, energy dependence for $n(E)$, taken from [22]; additionally, we introduce some overlap of the bins. We compare our results for the azimuthal dependence of the neutrinos to the dependence of the observed recoil electrons seen at Super-K, normalized to their no-oscillation Monte Carlo simulation. The results are pictured in Fig. 3. Though we do not model the recoil electron, there is a strong correlation between the two processes for the high-energy events. The results are encouraging. For the lower energies, all the solutions produce little electron neutrino oscillations as indicated by the data. However, there is a visible low-energy muon neutrino oscillation which is

larger in the theory than in the data. An improved model of the atmospheric data is required to better understand this. Most importantly, the high-energy muon zenith-angle data is qualitatively similar to the results given by our model.

In summary, within the model developed here of the neutrino oscillation data, we find that the region $\theta_{13} < 0$ plays an important role in understanding the oscillation parameters for three-neutrino oscillations. As oscillation probabilities for negative and positive values of θ_{13} are not simply related, the analysis cannot be done in terms of $\sin^2 \theta_{13}$. The work presented here is intended to motivate a more thorough and careful examination of the $\theta_{13} < 0$ region of the parameter space.

The authors are grateful for very helpful conversations with D. V. Ahluwalia and I. Stancu. This work is supported by the U.S. Department of Energy under grant No. DE-FG02-96ER40963.

- [1] M. Maiani, Phys. Lett. **B62**, 183 (1976).
- [2] J. Gluza and M. Zralek, Phys. Lett. **B517**, 158 (2001).
- [3] D. C. Latimer and D. J. Ernst, nucl-th/0405073.
- [4] B. T. Cleveland, et al., Astrophys. J. **496**, 505 (1998).
- [5] J. N. Abdurashitov, et al., Phys. Rev. C **60**, 055801 (1999); J. Exp. Theor. Phys. **95**, 181 (2002).
- [6] W. Hampel, et al., Phys. Lett. **B 447**, 127 (1999).
- [7] M. Altmann, et al., Phys. Lett. **B 490**, 16 (2000).
- [8] Q. R. Ahmad, et al., Phys. Rev. Lett. **87**, 071301 (2001); Phys. Rev. Lett. **89**, 011301 (2002).
- [9] S. N. Ahmed, et al., nucl-ex/0309004.
- [10] M. Apollonio, et al., Phys. Lett. **B 420**, 397 (1998); **B 466**, 415 (1999); Eur. Phys. J. **C 27**, 331 (2003).
- [11] K. Eguchi, et al., Phys. Rev. Lett. **90**, 021802 (2003).
- [12] Y. Fukuda, et al., Phys. Lett. **B335**, 237 (1994); **B433**, 9 (1998); **B436**, 33 (1998); Phys. Rev. Lett. **81**, 1562 (1998).
- [13] Y. Fukuda et al., Phys. Lett. **B436**, 33 (1998); Phys. Rev. Lett. **82**, 2644 (1999); **86**, 5651 (2001).
- [14] M. H. Ahn, et al., Phys. Rev. Lett. **90**, 041801 (2003).
- [15] C. Athanassopoulos, et al., Phys. Rev. Lett. **77**, 3082 (1996); Phys. Rev. C **54**, 2685 (1996); Phys. Rev. Lett. **81**, 1774 (1998); Phys. Rev. C **58**, (2489); A. Aguilar et al., Phys. Rev. D **64**, 112007 (2001).
- [16] B. Armbruster, et al., Phys. Rev. D **65**, 112001 (2002).
- [17] J. N. Bahcall, M. H. Pinsonneault, and S. Basu, Astrophys. J. **555**, 990 (2001).
- [18] L. Wolfenstein, Phys. Rev. D **17**, 2369 (1978); S. P. Mikheyev and A. Yu Smirnov, Sov. J. Nucl. Phys. **42**, 913 (1985).
- [19] M. C. Gonzalez-Garcia and Y. Nir, Rev. Mod. Phys. **75**, 345 (2003).
- [20] M. C. Gonzalez-Garcia and C. Peña-Garay, Phys. Rev. D **68**, 093003 (2003).
- [21] M. Maltoni, T. Schwetz, M. A. Tórtola, and J. W. F. Valle, Phys. Rev. D **68**, 113010 (2003).
- [22] M. Honda, T. Kajita, K. Kasahara, and S. Midorikawa, Phys. Rev. D **52**, 4985 (1995).